Electron transfer and bond-forming reactions following collisions of I^{2+} with CO and CS_2

James D. Fletcher, Michael A. Parkes and Stephen D. Price*

Department of Chemistry, University College London, 20 Gordon Street, London, WC1H 0AJ, UK

1 Abstract

Collisions between I^{2+} and CO have been investigated using time-of flight mass spectrometry at a range of centre-of-mass collision energies between 0.5 eV and 3.0 eV. Following I^{2+} + CO collisions we detect I^+ + CO^+ from a single-electron transfer reaction and IO^+ + C^+ from bond-forming reactivity. Reaction-window calculations, based on Landau-Zener theory, have been used to rationalise the electron transfer reactivity and computational chemistry has been used to explore the $[I\text{-}CO]^{2+}$ potential energy surface to account for the observation of IO^+. In addition, collisions between I^{2+} and CS_2 have been investigated over a range of centre-of-mass collision energies between 0.8 eV and 6.0 eV. Both single and double electron transfer reactions are observed in the I^{2+}/CS_2 collision system, an observation again rationalized by reaction-window theory. The monocations IS^+ and IC^+ are also detected following collisions of I^{2+} with CS_2, and these ions are clearly products from a bond-forming reaction. We present a simple model based on the structure of the $[I\text{-}CS_2]^{2+}$ collision complex to rationalize the significantly larger yield of IS^+ than IC^+ in this bond-forming process.

Corresponding author email: s.d.price@ucl.ac.uk

1 Introduction

A combined approach involving experiments and chemical modelling has indicated that the properties and chemistry of small multiply-charged ions, particularly dications, are relevant in a number of energised environments, such as plasmas, interstellar clouds and planetary ionospheres.[1-6] Such potential applicability has made the gas-phase bimolecular reactivity of atomic and molecular dications a focus of experimental investigations for a number of years. Single-electron transfer (SET) reactivity, which is close to ubiquitous in collisions of small dications with neutrals, has been extensively studied and is now reasonably well understood.[7-18] Specifically, the "reaction-window" concept, arising from an application of Landau-Zener theory to dication-neutral collisions, readily explains the SET reactivity in these encounters at low collision energies.[9-11,13,14,18-22] Scattering experiments, employing crossed-beam mass spectrometers, guided ion beams and coincidence techniques, have also been used to elucidate the detailed mechanisms of dicationic SET reactivity, usually revealing a direct pathway.[9,11,14,21-28] More recently, similar experiments have been performed to help understand the dynamics of double electron transfer (DET) reactions in dication-neutral collisions.[9] In parallel with these studies of dicationic electron transfer, laboratory studies have also revealed that molecular dications can take part in bond-forming reactivity at low collision energies in the centre-of-mass frame.[11,14,20,22,28-39] Indeed, it has been shown that gas-phase dication chemistry can provide new pathways for the formation of specific bonds and unusual compounds.[35,40]

Focusing on atomic dications, the reactive species in the current study, there has been considerable attention paid to the bond-forming chemistry of metal atom dications; such investigations were stimulated, in part, by an attempt to rationalise the activity of heterogeneous catalysts.[41] This interest in the chemistry of metallic dications was prompted by the observation that atomic transition metal dications exhibited varied and rich bond-forming chemistry following collisions with alkanes.[42-44] In contrast to metallic species, there has been far less attention paid to the bond-forming reactivity of non-metallic atomic dications with neutrals. Past experiments have focused predominantly on the bond-forming chemistry of the Ar^{2+} dication following collisions with various neutrals.[9,19,45-48] For example, collisions between Ar^{2+} with CO, CO_2, O_2 and N_2 form ArC^{2+}, ArO^{+}, ArO^{2+} and ArN^{2+}respectively, albeit with low yield.

In this paper we report the reactions that take place following collisions of doubly ionised atomic iodine (I^{2+}) with two small neutral molecules: carbon monoxide (CO) and carbon disulphide (CS_2). As well as observing electron transfer reactivity, in both of these collision systems we detect singly charged species generated by bond-forming reactions. Existing electrostatic models, in conjunction with *ab inito* electronic structure calculations, have been used to rationalise the behaviour we observe in these reactions of I^{2+}.

2 Experimental

The experimental apparatus used in this study has been described in detail in previous publications, therefore only a brief description is provided here.[49] In summary, monocations and multiply-charged cations are generated, from an appropriate precursor gas, in an electron ionisation source (~150 eV electrons). These positive ions are extracted from the source and accelerated to a potential of 250 V. The extraction voltage and source design ensure that the resulting ion beam has a small kinetic energy spread (0.5 eV). After acceleration, the ions enter a commercial velocity filter which selects the dication of interest according to its *m*/*z* value. The resulting mass-selected ion beam is decelerated to the chosen collision energy (typically less than 15 eV in the laboratory frame) and refocused. After this deceleration and focusing, the ion beam then passes through an effusive jet of reactant gas in the 'interaction' region of the experiment. The interaction region doubles as the source region of a linear time-of-flight mass spectrometer (TOFMS). The TOFMS is aligned perpendicularly to the direction of the reactant ion beam. The pressure in the interaction region is kept low (typically significantly less than 10^{-5} Torr) in order to ensure that single-collision conditions are maintained.[50] Relatively low collision energies were employed in this study in order to promote any bond-forming reactivity. The lowest collision energy is limited by maintaining a practical flux of dications, as the dication beam current decreases markedly with decreasing collision energy. Following the dication-neutral interactions, a pulse generator, running at 50 kHz, triggers the application of a positive voltage pulse to a repeller plate which accelerates all of the positively charged ions (reaction products and unreacted parent dications) from the interaction region into the acceleration region of the mass spectrometer and then into a field-free drift tube. At the end of the drift tube the ions impact upon a micro-channel plate detector. Signals from the detector are amplified, filtered by a constant-fraction discriminator and converted into arrival times by a time-to-digital converter (TDC). The start signal for the TDC is provided by a trigger from the pulse generator, sent shortly after the repeller plate is energised. The ionic flight times recorded by the TDC are sent to a PC, *via* a memory module, where they are stored as a histogram of counts as a function of TOF (a mass spectrum). Recording a single mass spectrum typically involves several thousand data acquisition cycles, where a single cycle involves collecting 64 kB of data. For each collision energy studied in this work one initial mass spectrum, comprising 10000 cycles, was gathered in order to ensure that even very weak ion signals were clearly identified. A further six pairs of spectra, each comprising 5000 cycles, were gathered at each collision energy for product ion intensity analysis. Each pair of mass spectra consists of a 'gas-on' spectrum, with the collision gas present, and a 'gas-off' spectrum, without the collision gas. In this study the reactant I^{2+} ions were formed by dissociative multiple ionisation of I_2 molecules taken from the vapour above a commercial, high purity, sample of solid iodine held at room temperature. The CO collision gas was a high-purity commercial sample and was used without further purification. The CS_2 sample

was taken from the vapour above a commercial liquid sample held at just below room temperature; the CS_2 was purified, before use, by several cool-pump-warm cycles.

A complementary computational study using GAUSSIAN-09[51] was carried out in an attempt to determine the structures and energetics of the products of the bond-forming reactions observed following the collisions of I^{2+} with CO and CS_2. Calculated energetics were combined with data from the literature[52] to determine the relative energies of the product asymptotes corresponding to the product ions that we detect experimentally. Zero point energy corrections at the MP2 level are included in all of our energetics. Additionally, the structures and relative energies of relevant intermediates and transition states were also determined computationally. In all cases single point energy calculations were performed using a CCSD(T)/aug-cc-pVTZ algorithm at optimised geometries obtained and characterized using an MP2(fc)/aug-cc-pVTZ procedure.

3 Reaction-window theory

In both of the I^{2+} collision systems we have investigated, we find that single electron transfer (SET) is the major contributor to the product ion yield. Reaction window (RW) theory has been used to calculate cross-sections for these electron transfer reactions to assist in rationalising our experimental findings. The methodology of our RW calculation has been described in detail in the literature,[12,49] and only a brief account is provided here. In the RW model, electron transfer occurs at the intersection (curve crossing) between reactant (dication + neutral) and product (monocation + monocation) potential energy curves, with the reactants and products pictured as structureless particles and the inter-species separation viewed as the reaction co-ordinate. The inter-species separation of the curve crossing, the crossing radius, can be determined by using appropriate functions to approximate the potential energy curves of the reactant and product states. For dication/neutral collisions, the reactant potential is modelled as purely the result of polarization-attraction, a robust assumption given the significant interspecies separations where reactive curve crossings occur. The potential curve for the singly-charged products is represented purely by electrostatic repulsion, with an energy offset to ensure the reactant and product states are separated by the appropriate exothermicity.

Given the above model potentials, Landau-Zener theory (equation (1)) is used to calculate the probability δ of remaining on the same diabatic potential energy curve as the collision system passes through the crossing radius.[53-55] The value of δ determines the probability P of SET (equation (2)) as, for successful SET, the collision system must pass through the curve crossing twice (on approach and separation) but change potential surfaces only once. Thus, the maximum possible value of P is 0.5. The magnitude of δ is influenced by the values of several quantities at the crossing radius: the coupling

between the potential curves H_{12}, the difference in the gradients of the potential curves $|V_1' - V_2'|$ and the relative radial velocity of the reactants $v_r(b)$. The model potential energy curves are used to calculate the crossing radius and $|V_1' - V_2'|$ and then a semi-empirical methodology, proposed by Olson, is used to estimate $|H_{12}|$.[56] Thus, using the model potentials, δ and P can to be calculated at a given collision energy for an encounter with an impact parameter b.

$$\delta = \exp\left(\frac{-\pi|H_{12}|^2}{2\hbar|V_1' - V_2'|v_r(b)}\right) \quad (1)$$

$$P = 2\delta(1-\delta) \quad (2)$$

To derive a value for the SET cross section at this given collision energy we then integrate P over all values of b (0 to b_{max}) for which the system passes through the crossing radius:

$$\sigma_{SET} = \int_0^{b_{max}} 2\pi b\, P(b)\, \mathrm{d}b \quad (3)$$

Since the value of δ decreases strongly as the radius of the curve crossing decreases, due to the increasing coupling between the reactant and product states, this model results in a range of interspecies separations, the so-called *reaction window*, over which SET is efficient. If the curve crossing is at too small an interspecies separation, the coupling is too strong ($\delta \rightarrow 0$, $P \rightarrow 0$) and an electron is transferred as the reactants approach and as the species separate, thus there is no net electron transfer. Conversely, if the curve crossing is at too large an interspecies separation, the coupling between the reactant and product states is too weak ($\delta \rightarrow 1$, $P \rightarrow 0$) for an electron to be transferred at all. Somewhere between these two limits lies the reaction window. Previous studies have indicated that for dicationic SET the reaction window lies between interspecies separations of approximately 3 Å and 6 Å. Given our simple potential model, such separations correspond approximately to SET exothermicities between 2 eV and 6 eV.[14,49] The above model has allowed the satisfactory rationalisation of dicationic SET in a number of different collision systems.[19,20,57] For collisions of I^{2+} with CO and CS_2, we have used this model to estimate the SET cross sections for populating the accessible electronic states of the product monocations to explain the reactivity we observe.

4 Results

Mass spectra were recorded, as described above, at centre-of-mass (CM) collision energies (T_{cm}) ranging from 0.5 eV to 3.0 eV for I^{2+}/CO and 0.8 eV to 6.0 eV for I^{2+}/CS_2. Product ions were identified by comparison of 'gas-on' and 'gas-off' spectra at each collision energy. The gas-off spectra were used to correct the product ion yields in the gas-on spectra for any impurities present in the reactant ion beam and for any contribution from reactions with the background gas in the collision region. For each

product ion, in order to quantify the ion yield, an average relative product ion signal R was determined by normalisation of the corrected product ion signal to the incident dication intensity. The raw product ion signal and R are both, of course, a function of the collision gas pressure. Hence, for consistency, the collision gas pressure was maintained at the same value for all the experiments.

Table 1: Experimental product ion signals R (relative to I^{2+}) for the product ions detected following I^{2+}/CO collisions as a function of CM collision energy T_{cm}.

T_{cm} /eV	10^4R			
	C^+ [a]	CO^+ [b]	I^+ [b]	IO^+ [a]
0.5	0.06	7.6	53.7	0.30
0.7	0.05	7.3	42.0	0.31
0.9	0.06	8.4	50.1	0.28
1.0	0.07	9.9	56.0	0.33
1.2	0.07	9.1	50.0	0.31
1.4	0.05	7.9	47.1	0.23
1.6	0.06	9.5	47.7	0.34
1.9	0.07	11.5	57.4	0.42
2.2	0.11	14.5	57.5	0.50
2.4	0.10	14.0	49.0	0.52
2.7	0.03	9.1	39.4	0.33
3.0	0.05	9.5	36.6	0.28

a Estimated uncertainty 20%
b Estimated uncertainty 4%

4.1 I^{2+} + CO

The product ions we observe following I^{2+}/CO collisions are listed in Table 1, where R values are also reported for each of the product ions at each collision energy. Table 1 also includes an estimate of the uncertainties in the R values. These uncertainties are estimated from both the reproducibility of individual measurements and an analysis of the uncertainty introduced by the subtraction of background signals. We see that I^+ and CO^+ ions are clearly the most abundant products, revealing a strong SET reaction (reaction (4)). Given that this SET reaction evidently dominates the reactivity, one would in principle expect the yields of I^+ and CO^+ to be approximately equal. However, Table 1 clearly shows that the I^+ ion signal is seven times more intense than the sum of the CO^+ and C^+ signals at T_{cm} = 0.5 eV. Furthermore, we can also clearly see in Table 1 that, while $R(CO^+)$ increases with increasing T_{cm}, $R(I^+)$ exhibits a gradual decrease. At T_{cm} = 2.2 eV, $R(I^+)$ is only four times greater than $R(CO^+)$.

$$I^{2+} + CO \rightarrow I^+ + CO^+ \qquad (4)$$

The intensity difference between the I^+ and CO^+ signals, and the changes seen with collision energy, are caused by significant differences in our experimental detection efficiency for ions derived from the

dication reactant (*i.e.* I^+) and ions derived from the neutral molecule (*i.e.* CO^+) in the SET reaction. These discrimination effects have been discussed extensively in previous publications.[19,20] Strong forward-scattering typically dominates the reaction dynamics in dicationic SET reactions, due to the electron transfer occurring at significant inter-species separations.[14,49] This form of scattering results in the I^+ products having CM velocities predominantly orientated in the direction of the initial CM velocity of I^{2+}, whilst the products derived from the neutral molecule (CO^+) have CM velocities predominantly orientated in the direction of the initial CM velocity of the neutral molecule. At the collision energies in our work, these CM scattering dynamics give the singly-charged products (I^+ and CO^+) distinctly different laboratory (LAB) frame velocity distributions.[14,49] The ions derived from the reactant dication possess significant LAB frame velocities, velocities markedly greater than the LAB velocity of the CM, and are termed 'fast' ions. In contrast, ions derived from the neutral molecule

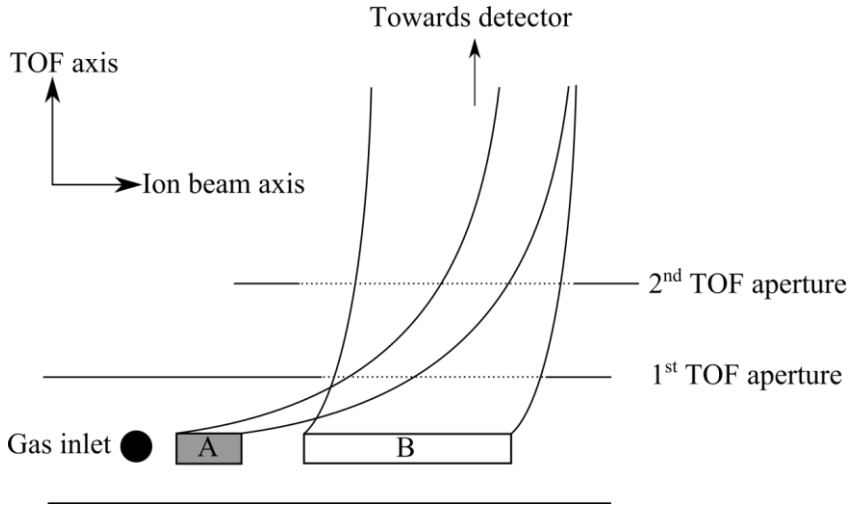

Figure 1: Schematic diagram of the TOF-MS interaction region illustrating the effect of a product ion's velocity on its detection efficiency for 'fast' (A) and 'slow' ions (B). See text for details.

have low LAB frame velocities, distinctly less than the velocity of the CM, and we term these species 'slow' ions. Our experimental geometry is optimized to collect the fast ions significantly more efficiently than the slow ions. This experimental geometry (Figure 1) involves the jet of neutral gas crossing the dication beam before the ion beam reaches the centre of the source region of the TOF-MS. At our collision energies, fast ions created in the interaction region pass efficiently (Figure 1) into the TOFMS and are detected. However, with this experimental arrangement, slow ions are sampled from a distinctly different volume of the interaction region to the fast ions. As illustrated in Figure 1, only slow ions formed considerably closer to the centre of the source region of the TOFMS will go on to reach the detector. The neutral gas pressure is markedly lower in this second region of the apparatus, as it is further from the gas jet, and thus fewer detectable CO^+ ions are formed.

We have calculated the I^+ and CO^+ product ion velocities using the known I^{2+} reactant velocity and by estimating the kinetic energy release following I^{2+}/CO collisions.[21-23] These product velocities, and the internal geometry of the mass spectrometer, are then used to estimate the detection efficiencies of the singly charged ions using the procedure previously outlined by Burnside *et al*.[19,20] As expected, the detection efficiency of I^+ greatly exceeds that of CO^+ at our low collision energies. Upon increasing collision energy, the I^+ detection efficiency steadily decreases as the sampled volume of the source region decreases in size. In contrast, as the CO^+ LAB frame velocity increases the detection efficiency for these ions also increases as the detected ions are sampled from regions of higher neutral gas pressure. This analysis clearly accounts for the variation in the I^+ and CO^+ signals with increasing collision energy (Table 1). For example, at T_{cm} = 2.2 eV the ratio of I^+ to CO^+ detection efficiencies given by the above analysis is approximately 4. Such a value for the relative detection efficiency of these product ions then indicates, given the experimental *R* values (Table 1), that the I^+ and CO^+ product ions are formed in equal numbers, as expected. Previous work, using the same experimental apparatus, yields results which show the same pattern of behaviour following Cl^{2+}/CO collisions.[19]

As illustrated in Figure 2, a clear signal corresponding to IO^+ is also observed following collisions of I^{2+} with CO. No signals corresponding to any other bond-forming reactivity (*e.g.* IC^+) are detected.

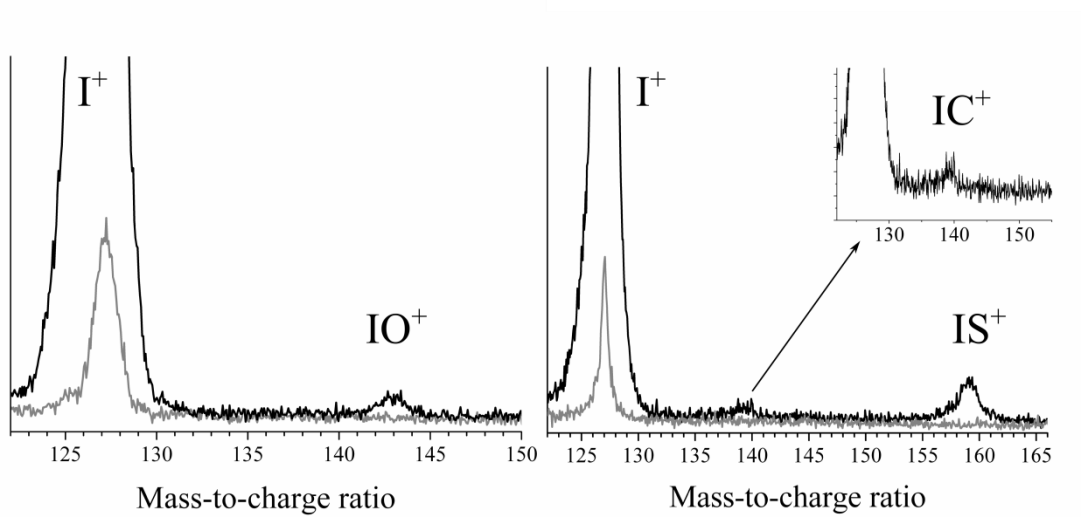

Figure 2: Representative mass spectra recorded following collisions of I^{2+}/CO (left) and I^{2+}/CS_2 (right) at T_{cm} = 3 eV and 6 eV respectively highlighting the signals due to the bond-forming reactions. In both cases the black line indicates a normalised "gas on" spectrum and the grey line indicates a normalised "gas off" spectrum, recorded at the same collision energy. The inset on the right panel shows the I^{2+}/CS_2 spectrum on enlarged horizontal and vertical scales in order to highlight the IC^+ peak at m/z = 139.

Given conservation of charge and mass, the ion that accompanies IO^+ formation must be C^+. Satisfyingly (Table 1) we also detect C^+ ions following collisions of I^{2+} with CO. The mechanism of this bond forming reaction is likely to involve the formation of a collision complex,[21,58] as discussed in detail below. This class of reaction dynamics results in effectively isotropic product scattering in the CM frame and the pairs of product ions which are formed are sampled from similar volumes in our apparatus. Therefore the detection efficiency of these product ions is determined largely by their velocity, which, in turn, is governed by their mass. Specifically, when a doubly-charged complex (*e.g.* $[I\text{-}CO]^{2+}$) fragments, the kinetic energy released is distributed between the two singly-charged products and the light products will be formed with greater energies than the heavier products. As a consequence of this energy distribution, a greater number of the light ions formed will be lost 'sideways' and not reach the detector. The heavier partner ions, formed in equal numbers, will therefore be detected more efficiently. This efficiency effect accounts for the markedly larger product ion signals for IO^+ than for the lighter partner C^+ ion (Table 1). Other possible sources of C^+ are dissociative SET and double electron transfer (DET); the yield of C^+ from these processes are discussed in detail below.

4.2 $I^{2+} + CS_2$

The product ions detected following I^{2+}/CS_2 collisions are listed in Table 2, where *R* values for each ion are also reported. As shown in Table 2, intense signals corresponding to CS_2^+ and I^+ are observed at all of the collision energies investigated. Again, $R(I^+)$ greatly exceeds $R(CS_2^+)$ revealing the same strong forward scattering dynamics following SET as discussed above. Furthermore, as well as CS^+, C^+ and S^+ fragments, a CS_2^{2+} signal is also observed which indicates that DET makes a significant contribution to the reactivity in I^{2+}/CS_2 encounters. The observation of DET following I^{2+} collisions with CS_2, but not following collisions with CO, is readily rationalized on energetic grounds. Specifically, DET is exothermic for I^{2+}/CS_2 collisions (ΔH_r = -3.8 eV), in contrast to the I^{2+}/CO collision system where it is markedly endothermic (ΔH_r = 12.8 eV).[52,59,60] Thus, DET between I^{2+} and CS_2 is expected to occur across the collision energy range of this work. The sampling volumes for the formation of CS_2^+ and CS_2^{2+} from SET and DET were calculated using the model described above. In calculating the product ion velocities we assume that DET has a negligible kinetic energy release. The model indicates both ions will be detected with approximately equal efficiency. Therefore, we conclude that, in this collision system, non-dissociative SET is the dominant reactive process, since $R(CS_2^+)$ is more than ten times larger than $R(CS_2^{2+})$ across the energy range of the study. These electron transfer processes are discussed further below.

Two product ions, IC^+ and IS^+, arising from bond-forming processes are detected throughout the collision energy range investigated in this study. The intensity of IS^+ is significantly greater than IC^+, as shown in Figure 2. These bond-forming products are likely to be formed *via* the dissociation of a short-lived $[ICS_2]^{2+}$ collision complex and, as mentioned above, the detection efficiency of a given

product ion formed in such a process is strongly influenced by its mass. Since IC^+ and IS^+ ions produced in bond forming reactions are much heavier than their partner ions, and we estimate that such heavy species will be detected with approximately equal efficiency. Therefore, we conclude that the IS^+/IC^+ intensity differences we observe broadly reflect the different reactive cross sections for the different bond-forming processes; an explanation for this propensity is discussed further below.

Table 2: Experimental relative product signals *R* (relative to I^{2+}) for the product ions detected following I^{2+}/CS_2 collisions as a function of CM collision energy T_{cm}.

T_{cm} /eV	10^4R							
	C^+ *c*	S^+ *b*	CS_2^{2+} *a*	CS^+ *b*	CS_2^+ *b*	I^+ *b*	IC^+ *a*	IS^+ *a*
0.7	5.1×10^{-3}	0.66	0.03	1.00	0.08	39.13	0.04	0.55
1.5	5.1×10^{-3}	0.80	0.06	1.12	0.20	24.24	0.05	0.49
2.2	7.4×10^{-3}	1.14	0.05	1.33	0.46	20.66	0.05	0.51
3.0	1.2×10^{-2}	1.60	0.12	1.78	2.00	19.53	0.09	0.53
3.7	1.7×10^{-2}	2.31	0.15	2.62	2.48	22.52	0.15	0.62
4.5	2.1×10^{-2}	3.70	0.25	5.01	1.73	25.58	0.15	0.67
5.2	1.9×10^{-2}	3.45	0.22	4.45	1.34	22.76	0.14	0.56
6.0	2.0×10^{-2}	3.74	0.24	4.75	7.64	22.01	0.15	0.62

a Estimated uncertainty 20%
b Estimated uncertainty 4%
c Estimated uncertainty 30%

Discussion

4.3 I^{2+} + CO collision system

4.3.1 Electron transfer reactivity

The energetic data taken from the literature for both SET and DET reactions relevant to the I^{2+}/CO collision system are summarised in Table 3.[52,60,61] The neutral reactant gas is admitted as an effusive jet, therefore only the ground ($X\ ^1\Sigma^+$) electronic state of the CO reactant will be populated. However, since we use 150 eV electrons to generate our dication beam, a number of I^{2+} excited states are energetically accessible. We certainly expect that the I^{2+} beam will be primarily composed of the ^4S ground state and perhaps the ^2D and ^2P excited states from the $I^{2+}(p^3)$ configuration.[62] The cross sections for populating higher-lying excited states of I^{2+} in the electron ionization source should drop off rapidly with the increasing energy of these excited states, and inspection shows that such higher energy states should have facile radiative relaxation pathways to the p^3 electronic states.[60] Supporting

this analysis, we see below that the reactivity we observe is satisfactorily explained assuming just the two lowest I^{2+} electronic states (^4S and ^2D) are present in our ion beam.

In this collision system a number of $I^+ + CO^+$ product states are accessible, the relevant combinations of reactant and product electronic states are listed in Table 3.[60,63]

Table 3**:** Calculated SET cross-sections σ_{SET}, in arbitrary units, for the population of various product states following I^{2+}/CO collisions at T_{cm} = 1.9 eV. Also listed are reaction enthalpies ΔH_r for the various channels. [52,60,63]

Electronic states of products		Electronic state of I^{2+} reactant[a]			
		X ^4S		A ^2D	
I^+	CO^+	ΔH_r /eV	σ_{SET}	ΔH_r /eV	σ_{SET}
X ^3P	X $^2\Sigma^+$	-5.1	0.8	-6.6	~0
A ^1D	X $^2\Sigma^+$	-3.4	28.0	-4.9	1.6
X ^3P	A $^2\Pi_i$	-2.6	3.3	-4.0	18.1
B ^1S	X $^2\Sigma^+$	-1.4	~0	-2.9	12.9
A ^1D	A $^2\Pi_i$	-0.8	~0	-2.3	1.0
X ^3P	B $^2\Sigma^+$	0.6	-	-0.9	~0
B ^1S	A $^2\Pi_i$	1.2	-	-0.3	~0

[a] The ^2D state of I^{2+} lies 1.5 eV above the ground state.[60]

For both the ^4S and ^2D states of the I^{2+} reactant, Table 3 shows the relevant energetics of the accessible product asymptotes and the calculated SET cross sections σ_{SET} for populating those asymptotes. The values of σ_{SET} are derived from the RW algorithm outlined above.[12,49]. The values of σ_{SET} shown in Table 3 indicate that three specific SET processes are responsible for the vast majority of the products of the non-dissociative SET reaction we observe in this collision system all three populating stable states of CO^+ .

$$I^{2+}(X\ ^4S) + CO(X\ ^1\Sigma^+) \rightarrow I^+(A\ ^1D) + CO^+(X\ ^2\Sigma^+) \quad (5)$$

$$I^{2+}(A\ ^2D) + CO(X\ ^1\Sigma^+) \rightarrow I^+(B\ ^1S) + CO^+(X\ ^2\Sigma^+) \quad (6)$$

$$I^{2+}(A\ ^2D) + CO(X\ ^1\Sigma^+) \rightarrow I^+(X\ ^3P) + CO^+(A\ ^2\Pi_i) \quad (7)$$

We note that spin is not conserved in reaction (5) and this reaction might perhaps be disfavoured with respect to reactions (6) and (7). However, previous work has shown that increased spin-orbit (SO) coupling, caused by the presence of heavy atoms such as iodine, can relax spin conservation in ionic

reactions and facilitate reactive processes which are nominally spin-forbidden, allowing them to occur efficiently.[64-66] Indeed, as shown below, the available non-dissociative SET reactions in the I^{2+}/CS_2 collision system are all spin allowed. Hence, the broadly comparable yields of I^+ from collisions with CO and with CS_2 that we observe (Table 1 and Table 2) perhaps hint that spin conservation is not restricting the non-dissociative SET reactivity of the ground state of I^{2+} in reactions with CO.

Considering the C^+ ions we detect (Table 1), these ions must accompany the formation of IO^+ but could also, in principle, be formed by dissociative SET or DET. We note this C^+ signal from reactions of I^{2+} with CO is strikingly smaller than the other ET product signals (Table 1). C^+ signals from dissociation of CO^{2+} ions formed by DET can be ruled out because, as discussed above, DET is significantly endothermic (ΔH_r = 12.8 eV) in this collision system, even allowing for the presence of excited $I^{2+}(p^3)$ states in the reactant beam.[52,61] Indeed, there is no additional experimental evidence for the occurrence of DET, such as an O^+ or CO^{2+} signal (CO^{2+} is metastable but with sufficient lifetime to be detectable in our experiment). SET reactions which populate high-lying dissociative states of CO^+ are strongly endothermic from the p^3 manifold of I^{2+}, as the lowest dissociative electronic state of CO^+ ($E\ ^2\Sigma$) lies 9 eV above the ground state.[63] Therefore, we conclude that bond-forming reactivity must account for all of the observed C^+ signal. The C^+ ion intensity we observe is smaller (by about a factor of 5) than that of IO^+. However, this relative intensity difference is undoubtedly due to the larger detection efficiency of the heavy products (IO^+ in this case) from bond-forming reactions, as discussed above.

If, as we conclude above, the bond-forming reaction is the dominant source of C^+ then we would expect the ratio $R(C^+)/R(IO^+)$ to remain effectively constant, or vary slowly, over the range of collision energies studied; a slow variation being a result of changes in the relative collection efficiency of the two product ions. We can extract the $R(C^+)/R(IO^+)$ ratio from the data presented Table 1 (See Supplementary Information, Figure S1). Satisfyingly, this analysis shows that, within the error limits given in Table 1, $R(C^+)/R(IO^+)$ decreases very slightly over the collision energy range studied, in accord with our conclusion that the bond-forming reaction is the only source of both IO^+ and C^+. The absence of any contribution from SET to the C^+ signal shows that the SET reactivity in this collision system is exclusively non-dissociative. This analysis also supports the conclusion than no highly excited states of I^{2+} are present in the reactant beam.

4.3.2 Bond-forming reactivity

As described above, we detect IO^+ across the range of I^{2+}/CO collision energies investigated in this work (Table 1). The yield of IO^+ is approximately 100 times smaller than the yield of I^+ from SET. We see that there is little change in $R(IO^+)$ as T_{cm} increases, this relative independence of the yield of

bond-forming reactions to small changes in T_{cm} has been noted before.[19,20,34] The observation of IO^+ can be rationalised using a model for dication/neutral reactions developed by Herman.[14] This model considers the competition between electron transfer and bond-forming processes, highlighting the importance of a collision complex on the route to the formation of new chemical bonds. Following Herman, [14] schematic potential energy surfaces (PESs) for a typical dication/neutral collision system are shown schematically in Figure 3, where the dication is I^{2+} and the neutral is a diatomic molecule XY.

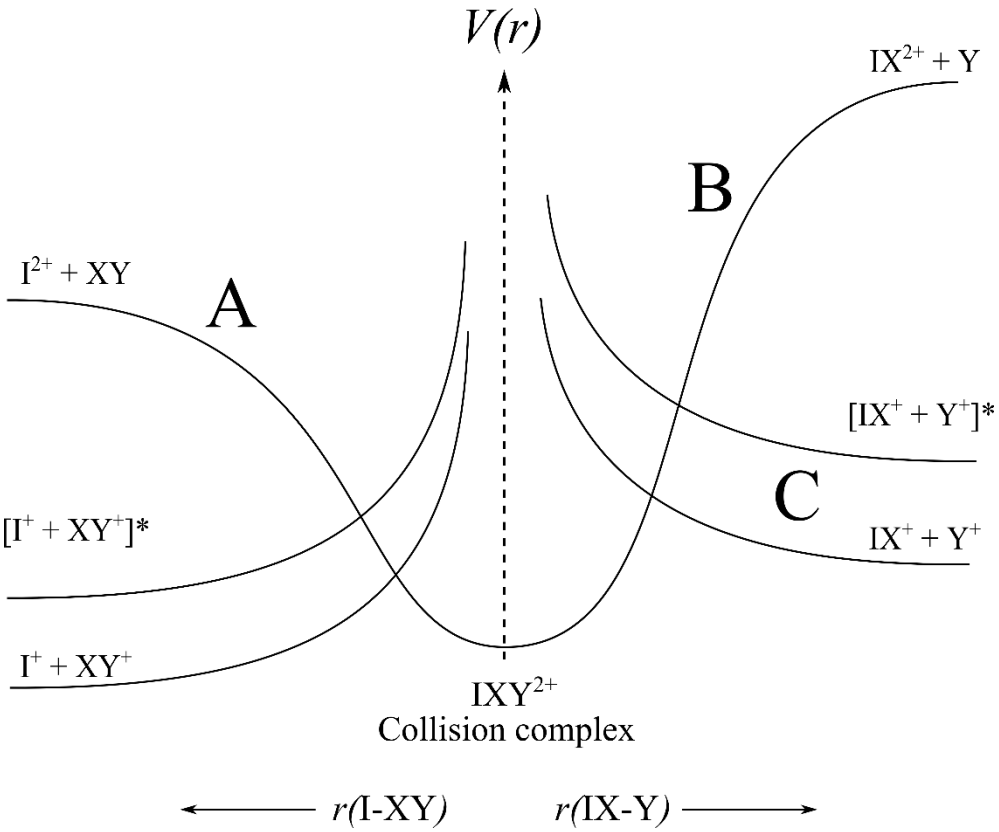

Figure 3**:** Schematic potential energy surfaces for rationalizing bond-forming reactivity in dication/neutral collision systems. See text for details.

As shown in Figure 3, the I^{2+} + XY PES is dominated by polarisation attraction (curve A). As the reactants approach each other they encounter a number of curve crossings which lead to single electron transfer. If the collision system does not cross onto these electron transfer surfaces the reactants can associate to form a collision complex. As described above, for the I^{2+}/CO collision system, many of these SET product curves lie within the theoretical reaction window, hence there is a significant probability of SET occurring. This conclusion is clearly demonstrated in the experimental results given in Table 1, where SET dominates the product ion yield. The collision complex can, of course, back-dissociate without rearrangement. The separating reactants then have another opportunity to cross onto

surfaces leading to SET products. Alternatively, again as shown in Figure 3, the collision complex can separate along a new reaction coordinate, to yield bond-forming products with different connectivity (*e.g.* IX^{2+} + Y, Figure 3, curve B). As the new products separate they will encounter a number of different curve crossings allowing access to product asymptotes involving pairs of monocations, such as IX^{+} + Y^{+} (Figure 3, curve C). The asymptotes for forming these pairs of monocations are typically markedly lower in energy than the IX^{2+} + Y asymptote (Figure 3). This energetic arrangement means that the ET curve crossings in the exit channel typically occur at small interspecies separations where the electronic coupling is strong. This strong coupling favours the population of the most exothermic product asymptotes for bond-forming reactivity, as the system only passes through these crossings in the exit channel once, as the products separate. Thus, we expect the majority of trajectories passing into the exit channel to form a pairs of monocations, again as observed experimentally

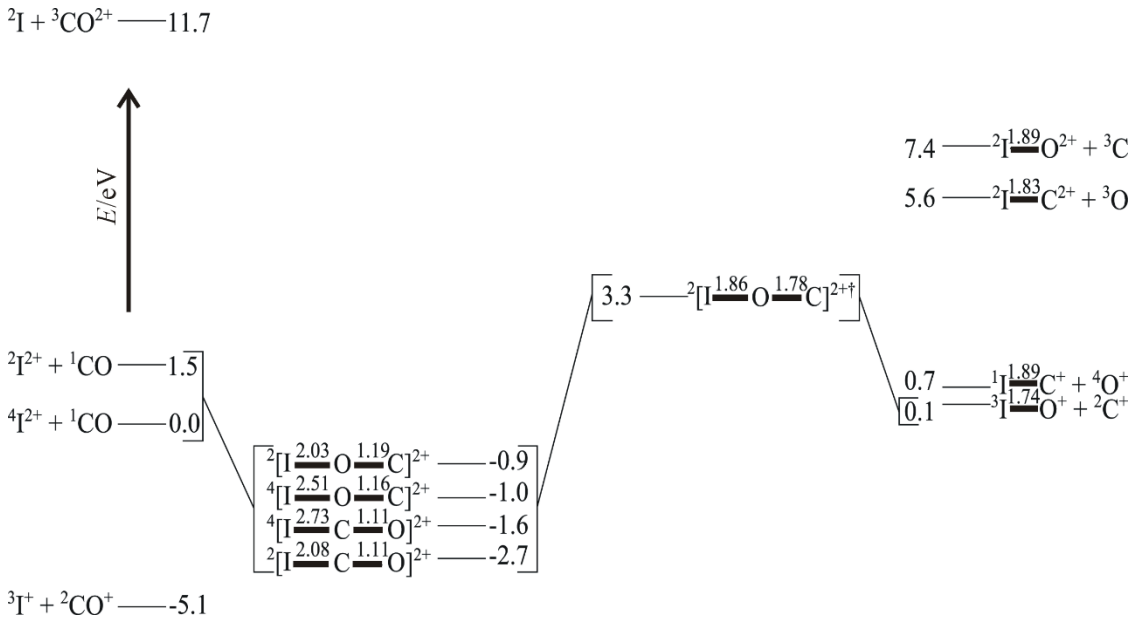

Figure 4**:** Calculated stationary points and product asymptotes on the I^{2+} + CO potential energy surface. See text for details. Energies (in eV) are expressed relative to the (^{4}S) I^{2+} + ^{1}CO asymptote. All species are linear and the bond-lengths are given in Ångstroms. Literature energetic data for electron transfer processes are indicated on the left-hand side of the diagram.[52,61]

As described above, we have explored the I^{2+}-CO PES using computational chemistry. The stationary points we have located in this exploration strongly indicate that the schematic model, described above, satisfactorily represents this collisional encounter (Figure 4). A number of viable structures for collision complexes have been located, at energies below the reactant asymptote, and these structures are shown in Figure 4. The ground and first excited states of the I^{2+} reactant are also

included in Figure 4. Additionally, Figure 4 shows the thermodynamic asymptotes for the possible bond-forming reaction products following I^{2+}/CO collisions; these relative energetics again were determined computationally. The SET and DET asymptotes, the energetics of which were taken from literature sources, are also included in Figure 4 for comparison.[52,60,61,63]

The above calculations show that the product asymptotes for forming $IC^+ + O^+$ and $IO^+ + C^+$ lie much lower in energy than the asymptotes for forming the dicationic products, IC^{2+} and IO^{2+}, as predicted above. Thus, again as explained above, we would expect the majority of flux in the exit channel of the bond-forming region of the PES to form monocationic products, as we observe experimentally. However, of the potential iodine containing products of this bond-forming process (IO^+ and IC^+) we only observe IO^+. Formation of $IO^+ + C^+$ is the most exothermic bond-forming channel (Figure 4). This channel is exothermic for the excited state I^{2+} reactant, which we expect to be present in the beam, but for the ground state of I^{2+} the formation of IO^+ is nominally endothermic and requires the involvement of the collision energy to take place. Considering the coupling arguments presented above, we would expect most of the bond-forming flux to arrive at the $IO^+ + C^+$ asymptote, as we observe experimentally. However, it seems surprising that no IC^+ is observed when this channel is just 0.4 eV more endothermic than the formation of $IO^{+\cdot}$ The experimental data therefore suggests that the $IC^+ + O^+$ asymptotes, although thermodynamically available (if one allows for the participation of the collision energy), are in some way dynamically inaccessible. To test this hypothesis we have performed further electronic structure calculations in order to search for transition states linking the collision complexes shown in Figure 4 to the $IO^+ + C^+$ and $IC^+ + O^+$ product asymptotes. As shown in Figure 4, a linear structure has been determined for $^2[IOC]^{2+\dagger}$, a transition state which is found to lie approximately 3 eV above the reactants in their ground states. Structures for $^4[IOC]^{2+\dagger}$, $^4[ICO]^{2+\dagger}$ and $^2[ICO]^{2+\dagger}$ were also found lying significantly higher in energy than $^2[IOC]^{2+\dagger}$. However, reliable energetic data cannot be reported for these latter three transition states as diagnostic tests revealed that these stationary points require multi-configuration wavefunctions for their full description, calculations beyond the scope of this work. Nevertheless, our calculations do indicate that the lowest accessible transition state leads to the formation of IO^+, transition states allowing the formation of IC^+ probably lie markedly higher in energy and could well be inaccessible at our collision energies. As such, this analysis readily explains our observation of only IO^+ as a bond-forming product. As discussed above, we expect spin conservation restrictions to be relaxed in this collision system due to significant spin-orbit coupling. Hence, we suggest that the $^2[IOC]^{2+\dagger}$ transition state can perhaps be formed following collisions between both ground and excited (p^3) states of I^{2+} with ground state CO, and both these interactions can result in the formation of IO^+.

4.4 I^{2+} + CS_2 collision system

4.4.1 Electron transfer reactivity

We detect both CS_2^+ and CS_2^{2+} ions following I^{2+}/CS_2 collisions, an observation which indicates both SET and DET are occurring in this collision system. Considering the SET reactivity, we have again used the RW model to rationalize which product states can be populated by SET. Table 4 lists the SET product asymptotes relevant to the I^{2+}/CS_2 collisions, along with the relevant energetic data and calculated values of the SET cross section σ_{SET}; the latter again considering the population of both the ground and first excited states of I^{2+}.[52,60,67,68]

Table 4: Reaction window calculations of SET cross-sections σ_{SET}, in arbitrary units, calculated following I^{2+}/CS_2 collisions. The cross-sections listed are calculated at T_{cm} = 3.7 eV. We do not observe a significant change of σ_{SET} as a function of collision energy.[52,60,67,68]

Electronic states of products		Electronic state of I^{2+} reactant			
		X ^{4}S		A ^{2}D	
I^+	CS_2^+	ΔH_r /eV	σ_{SET}	ΔH_r /eV	σ_{SET}
X ^{3}P	X $^2\Pi_g$	-9.1	2.4	-10.5	2.2
A ^{1}D	X $^2\Pi_g$	-7.3	3.7	-8.8	2.5
X ^{3}P	A $^2\Pi_u$	-6.3	6.3	-7.7	3.3
B ^{1}S	X $^2\Pi_g$	-5.4	11.7	-6.8	4.8
X ^{3}P	B $^2\Sigma_u^+$	-4.7	20.5	-6.1	7.1
A ^{1}D	A $^2\Pi_u$	-4.5	22.1	-6.0	7.6
X ^{3}P	C $^2\Sigma_g^+$	-3.1	26.3	-4.5	23.8
A ^{1}D	B $^2\Sigma_u^+$	-2.9	23.0	-4.4	25.5
B ^{1}S	A $^2\Pi_u$	-2.6	9.5	-4.0	32.1
A ^{1}D	C $^2\Sigma_g^+$	-1.3	~0	-2.8	16.0
B ^{1}S	B $^2\Sigma_u^+$	-1.0	~0	-2.4	4.6
B ^{1}S	C $^2\Sigma_g^+$	0.6	-	-0.8	~0

The σ_{SET} values listed in Table 4 show that, in this collision system, SET populates both the ground states and a number of excited states of CS_2^+ (X $^2\Pi_g$, A $^2\Pi_u$, B $^2\Sigma_u^+$ and C $^2\Sigma_g^+$)and I^+ (X ^{3}P, A ^{1}D and B ^{1}S). The X $^2\Pi_g$, A $^2\Pi_u$ and B $^2\Sigma_u^+$ states of CS_2^+ are all stable,[69,70] therefore any CS^+ or S^+ ions formed *via* SET must originate from the C $^2\Sigma_g^+$ state, which the RW model predicts will also be populated. Photoionisation studies have shown that (C $^2\Sigma_g^+$) CS_2^+ can fragment to form either CS^+ + S or S^+ + CS, with approximately equal probability, which is in line with our observations in Table

2.[69,70] States of CS_2^+ that lie higher in energy than C $^2\Sigma_g^+$ will not be populated as they are energetically inaccessible, consequently we do not observe any S_2^+ ions, which can only be formed *via* the dissociation of these higher-lying excited states.[69,70] We do observe C^+, but again the states of CS_2^+ which form this ion are also inaccessible to SET, even if the contribution of collision energy and the population of the p^3 excited states of the dication are considered. Satisfyingly, in accord with the above analysis, we will show below that the major source of C^+ is the bond-forming reactions of I^{2+} with CS_2. [69,70]

We detect CS_2^{2+} following collisions of I^{2+} with CS_2 as the double ionisation energy of CS_2 is 27.2 ± 0.2 eV, and DET is therefore exothermic.[59] As described above, our model of the product ion velocities indicates that CS_2^{2+} and CS_2^+ are detected with approximately equal efficiency and, since $R(CS_2^+)$ is substantially greater than $R(CS_2^{2+})$, we conclude that SET is the dominant ET process, although the contribution of DET to the ion yield is still significant. Previous studies of dication/molecule collision systems have explored the mechanism of DET in some detail.[9,71] The tentative conclusions of this earlier work were that in the DET process two electrons are transferred in a single step at the intersection of $X^{2+} + Y$ and $X + Y^{2+}$ reactant and product potentials. Experimental data indicates that efficient crossing radii for this DET process appear to lie between 2 Å and 3 Å.[71]

Table 5: Calculated crossing radii for DET reactions following I^{2+}/CS_2 collisions.

Electronic states of products		Electronic state of I^{2+} reactant			
I	CS_2^{2+}	X ^{4}S		A ^{2}D	
		ΔH_r /eV	$R_{CROSSING}$ /Å	ΔH_r /eV	$R_{CROSSING}$ /Å
X ^{2}P	X $^3\Sigma_g^-$	-2.4	2.8	-3.8	2.4
X ^{2}P	a $^1\Delta_g$	-1.6	2.9	-3.1	2.5
X ^{2}P	b $^1\Sigma_g^+$	-1.0	3.3	-2.4	2.6
X ^{2}P	c $^1\Sigma_u^-$	0.2	-	-1.2	3.0

We have used literature data to calculate the reaction exothermicities for DET in the I^{2+}/CS_2 collision system (Table 5).[52,59] We find that the exothermicities of energetically accessible product combinations range from 1.0 to 3.8 eV. These energetic calculations allow for the population of the A(^{2}D) state of I^{2+} in the ion beam, as well as the ground state of I^{2+}. DET reactions forming neutral iodine in anything other than the ground state are endothermic so are not included in this analysis. Using these exothermicities, and a simple electrostatic model for the product and reactant PESs, we are able to calculate the interspecies separations at which the reactant and product surfaces for DET intersect (the 'crossing radius'). We find that this model gives crossing radii for DET between 2.4 and 3.3 Å in the I^{2+}/CS_2 collision system. These crossing radii are comparable to those which allow efficient DET in the previously investigated O_2^{2+}/COS and O_2^{2+}/CS_2 systems, and again support the idea that in dicationic DET the two electrons are transferred in a single step.[71] The product PESs corresponding to the X $^3\Sigma_g^-$, a $^1\Delta_g$, b $^1\Sigma_g^+$ and c $^1\Sigma_u^-$ states of CS_2^{2+} all intersect the reactant curves within the empirical RW for

DET, therefore we could reasonably expect them all to be populated.[70] Although these low-lying states of CS_2^{2+} all lie energetically above the $CS^+ + S^+$ asymptote, the X state is metastable, thus a CS_2^{2+} is observed in the product mass spectra.[72] We cannot disentangle the contributions of dissociative SET and DET to the singly-charged fragment ion signals (CS^+, S^+ and C^+) but the vast majority of CS_2^{2+} ions formed in excited states are likely to dissociate to form $CS^+ + S^+$.[72] As stated above, the absence of any S_2^+ signal (Table 2) supports the above analysis of the DET process. The S_2^+ ions is minor product of the dissociation of the d $^3\Sigma_u^-$ state of CS_2^{2+} (forming $S_2^+ + C^+$) and this higher lying excited state of the dication is clearly not populated, in agreement with our cross-section calculations. The three body dissociation channels of CS_2^{2+} ($S^+ + S^+ + C$ and $S + S^+ + C^+$) are also likely to be extremely weak as both originate from higher excited states of the CS_2 dication. Therefore, since, $R(C^+)$ is of the same order as $R(IC^+)$ and $R(IS^+)$ we again conclude that bond-forming reactivity accounts for the majority of C^+ that we detect, having already ruled out a contribution from dissociative SET above. In contrast, the CS^+ and S^+ fragment ion signals will contain contributions from both dissociative electron transfer and bond-forming reactivity.

4.4.2 Bond-forming reactivity

We detect IC^+ and IS^+ following I^{2+}/CS_2 collisions across the range of T_{cm} studied in this work. No significant change in intensity of either species is observed with variation in T_{cm} over the collision energy range studied. Again, as rationalized above, the bond-forming products are monocations. The energies of the relevant bond-forming product asymptotes are listed in Table 6.

Table 6**:** Reaction exoergicities of selected bond-forming processes following I^{2+}/CS_2 collisions relative to the two populated states of I^{2+} in the ion beam. The reactant $^1CS_2$ is in the ground state. The energetics were obtained from both literature energetics and computational chemistry.[52,59,60,73]

Bond-forming reaction products	ΔH_r /eV	
	(^{4}S) I^{2+}	(^{2}D) I^{2+}
$^1IC^+ + {}^2S_2^+$	-7.3	-8.7
$^3IS^+ + {}^2CS^+$	-6.8	-8.2
$^1IS^+ + {}^2CS^+$	-6.0	-7.5
$^3IC^+ + {}^2S_2^+$	-4.9	-6.3
$^1IC^+ + {}^4S^+ + {}^3S$	-1.8	-3.2
$^2IS^{2+} + {}^3CS$	-1.4	-2.9
$^2IC^{2+} + {}^3S_2$	2.0	0.6

The relative energetics of IC and IS species, as well as their single and double ionisation energies, have been calculated using the computational methodology outlined above. Energetic data concerning the other products were obtained from the literature.[52,59,60,73] Table 6 clearly shows that the lowest lying bond-forming asymptotes are $^{1}IC^{+} + {}^{2}S_2^{+}$ and $^{3}IS^{+} + {}^{2}CS^{+}$. As explained in our analysis of the bond-forming reactivity in the I^{2+}/CO collision system, if the collision complex separates along the bond-forming co-ordinate it should predominantly populate the low-lying product asymptotes, involving IC^{+} and IS^{+} rather than IC^{2+} and IS^{2+}, just as we observe. However, given that we do not observe any S_2^{+} and $R(IS^{+}) > R(IC^{+})$ (Table 2), clearly a markedly greater proportion of the bond-forming trajectories reach the slightly less exothermic $IS^{+} + CS^{+}$ asymptote than the $IC^{+} + S_2^{+}$ asymptote. This disfavouring of the $IC^{+} + S_2^{+}$ asymptote can be accounted for qualitatively, as formation of $S_2^{+} + IC^{+}$ clearly requires a far more involved rearrangement of the reactants than the formation of CS^{+}, which is formed together with IS^{+}. Indeed, since we detect no S_2^{+} ions, it is clear that the $IC^{+} + S_2^{+}$ asymptote is inaccessible and thus IC^{+} must be formed together with S^{+}+ S. Since the $IC^{+} + S^{+}$ + S asymptote is considerably less exothermic than $IS^{+} + CS^{+}$, we then expect the crossing onto the $IS^{+} + CS^{+}$ asymptote to be the favoured bond-forming process as observed experimentally. To help further support this explanation of the bond-forming reactivity in the I^{2+}/CS_2 collision system we have again used computational chemistry to identify stationary points on the I^{2+}/CS_2 PES, using the methodologies and basis sets outlined above. A doublet $[I\text{-}CS_2]^{2+}$ complex was located which satisfactorily supports our explanation of the bond-forming reactivity given above. No quartet structures could be found, but, as explained above, the relaxation of spin selectivity, caused by the presence of the heavy I atom, means that it is viable to form this complex following collisions between CS_2 and both the ^{4}S ground state and the ^{2}D first excited state of I^{2+}. The structure of the collision complex is illustrated in Figure 5. Both I-S and I-C interactions are present in this $[I\text{-}CS_2]^{2+}$ complex, but clearly it is dynamically less elaborate for the complex to fragment to yield $IS^{+} + CS^{+}$ than to form $IC^{+} + S_2^{+}$.

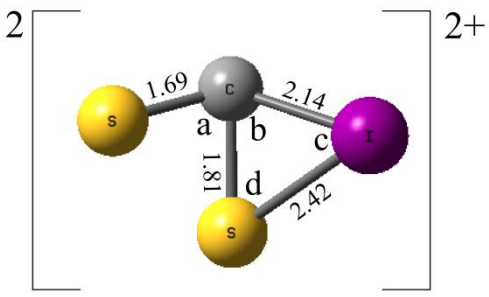

Figure 5: Structure of the collision complex located on the $^{2}[I\text{-}CS_2]^{+}$ potential energy surface. See text for details. Bond lengths are given in Ångstroms. Bond angles: (a) 78°; (b) 75°; (c) 46° (d) 59°.

5 Conclusions

We have studied the collisions of the atomic dication of iodine with neutral species for the first time, using a crossed-beam mass spectrometer. Reactions with CO and CS_2 both result in bond-forming processes as well as electron transfer. We can readily explain our observations using a simple electrostatic model of dication-neutral interactions coupled with electronic structure calculations. Electron transfer is the dominant reactive process in both of the collision systems, and the products we observe can be rationalized using reaction-window calculations. Chemical reactivity to form monocationic products of the form IX^+ makes a small, but not insignificant, contribution to the overall reactivity. In the case of I^{2+}/CO we see that only IO^+ is formed and our analysis indicates IC bonds cannot be formed in the collision energy range we have studied. For I^{2+}/CS_2, the relative yields of IC^+ and IS^+ appear to be determined largely by the structure of the accessible collision complex.

6 Acknowledgements

Financial support from UCL Impact Scheme for JDF is gratefully acknowledged. The authors acknowledge the use of the UCL *Legion* High Performance Computing Facility (Legion@UCL), and associated support services, in the completion of this work.

7 References

[1] Gronoff, G., Lilensten, J., Simon, C., Witasse, O., Thissen, R., Dutuit, O. and Alcaraz, C., 2007, *Astron. Astrophys.*, **465,** 641-5.

[2] Lilensten, J., Witasse, O., Simon, C., Soldi-Lose, H., Dutuit, O., Thissen, R. and Alcaraz, C., 2005, *Geophys. Res. Lett.*, **32,** L03203.

[3] Thissen, R., Witasse, O., Dutuit, O., Wedlund, C. S., Gronoff, G. and Lilensten, J., 2011, *Phys.Chem.Chem.Phys.*, **13,** 18264-87.

[4] Petrie, S. and Bohme, D. K., 2007, *Mass Spec. Rev.*, **26,** 258-80.

[5] Ricketts, C. L., Schroder, D., Alcaraz, C. and Roithova, J., 2008, *Chem-Eur.J.*, **14,** 4779-83.

[6] Pupyshev, A. A. and Semenova, E. V., 2001, *Spectroc. Acta Pt. B-Atom. Spectr.*, **56,** 2397-418.

[7] Parkes, M. A., Lockyear, J. F., Schroder, D., Roithova, J. and Price, S. D., 2011, *Phys. Chem. Chem. Phys.*, **13,** 18386-92.

[8] Žabka, J., Ricketts, C. L., Schröder, D., Roithová, J., Schwarz, H., Thissen, R., Dutuit, O., Price, S. D. and Herman, Z., 2010, *J. Phys. Chem. A*, **114,** 6463-71.

[9] Parkes, M. A., Lockyear, J. F. and Price, S. D., 2009, *Int. J. Mass Spectrom.*, **280,** 85-92.

[10] Lockyear, J. F., Parkes, M. A. and Price, S. D., 2009, *J. Phys. B: At. Mol. Opt. Phys.*, **42,** 145201.

[11] Ricketts, C. L., Schroder, D., Roithova, J., Schwarz, H., Thissen, R., Dutuit, O., Zabka, J., Herman, Z. and Price, S. D., 2008, *Phys. Chem. Chem. Phys.*, **10,** 5135-43.

[12] Rogers, S. A., Price, S. D. and Leone, S. R., 1993, *J. Chem. Phys.*, **98,** 280-9.

[13] Roithová, J., Žabka, J., Hrušák, J., Thissen, R. and Herman, Z., 2003, *J. Phys. Chem. A*, **107,** 7347-54.

[14] Herman, Z., 1996, *Int. Rev. Phys. Chem.*, **15,** 299 - 324.

[15] Ehbrecht, A., Mustafa, N., Ottinger, C. and Herman, Z., 1996, *J. Chem. Phys.*, **105,** 9833-46.

[16] Champkin, P., Kaltsoyannis, N. and Price, S. D., 1998, *Int. J. Mass Spectrom. Ion Proc.*, **172,** 57-69.

[17] Manning, M., Price, S. D. and Leone, S. R., 1993, *J. Chem. Phys.*, **99,** 8695-704.

[18] Herman, Z., 2013, *Mol. Phys.*, **111,** 1697-710.

[19] Burnside, P. W. and Price, S. D., 2007, *Phys. Chem. Chem. Phys.*, **9,** 3902-13.

[20] Burnside, P. W. and Price, S. D., 2006, *Int. J. Mass Spectrom.*, **249-250,** 279-88.

[21] Mrázek, L., Žabka, J., Dolejšek, Z., Hrušák, J. and Herman, Z., 2000, *J. Phys. Chem. A*, **104,** 7294-303.

[22] Herman, Z., Žabka, J., Dolejšek, Z. and Fárník, M., 1999, *Int. J. Mass Spectrom.*, **192,** 191-203.

[23] Dolejšek, Z., Fárník, M. and Herman, Z., 1995, *Chem. Phys. Lett.*, **235,** 99-104.

[24] Lockyear, J. F., Parkes, M. A. and Price, S. D., 2009, *J.Phys.B.*, **42**.

[25] Hu, W. P., Harper, S. M. and Price, S. D., 2005, *Molecular Physics*, **103,** 1809-19.

[26] Harper, S. M., Hu, S. W. P. and Price, S. D., 2004, *J. Chem. Phys.*, **120,** 7245-8.

[27] Hadjar, O., Ascenzi, D., Bassi, D., Franceschi, P., Sabidò, M. and Tosi, P., 2004, *Chem. Phys. Lett.*, **400,** 476-80.

[28] Roithova, J. and Schröder, D., 2007, *Phys. Chem. Chem. Phys.*, **9,** 2341-9.

[29] Dutuit, O., Carrasco, N., Thissen, R., Vuitton, V., Alcaraz, C., Pernot, P., Balucani, N., Casavecchia, P., Canosa, A., Picard, S. L., Loison, J.-C., Herman, Z., Zabka, J., Ascenzi, D., Tosi, P., Franceschi, P., Price, S. D. and Lavvas, P., 2013, *Astrophys. J. Suppl. S.*, **204,** 20.

[30] Lockyear, J. F., Ricketts, C. L., Parkes, M. A. and Price, S. D., 2010, *Chem. Sci.*

[31] Ricketts, C. L., Harper, S. M., Hu, S. W.-P. and Price, S. D., 2005, *J. Chem. Phys.*, **123,** 134322.

[32] Lambert, N., Kaltsoyannis, N., Price, S. D., Žabka, J. and Herman, Z., 2005, *J. Phys. Chem. A*, **110,** 2898-905.

[33] Roithová, J., Ricketts, C. L., Schröder, D. and Price, S. D., 2007, *Angew. Chem. Int. Ed.*, **46,** 9316-9.

[34] Tafadar, N. and Price, S. D., 2003, *Int. J. Mass Spectrom.*, **223–224,** 547-60.

[35] Lockyear, J. F., Parkes, M. A. and Price, S. D., 2011, *Angewandte Chemie International Edition*, **50,** 1322-4.

[36] Ascenzi, D., Aysina, J., Zins, E.-L., Schroeder, D., Zabka, J., Alcaraz, C., Price, S. D. and Roithova, J., 2011, *Phys. Chem. Chem. Phys.*, **13,** 18330-8.
[37] Levee, L., Calogero, C., Barbieri, E., Byrne, S., Donahue, C., Eisenberg, M., Hattenbach, S., Le, J., Capitani, J. F., Roithova, J. and Schroeder, D., 2012, *Int. J. Mass Spectrom.*, **323,** 2-7.
[38] Shaffer, C. J., Schroeder, D., Roithova, J., Zins, E.-L., Alcaraz, C., Zabka, J., Polasek, M. and Ascenzi, D., 2013, *Int. J. Mass Spectrom.*, **336,** 17-26.
[39] Vachelova, J. and Roithova, J., 2012, *Int. J. Mass Spectrom.*, **311,** 51-5.
[40] Ascenzi, D., Tosi, P., Roithova, J., Ricketts, C. L., Schroder, D., Lockyear, J. F., Parkes, M. A. and Price, S. D., 2008, *Phys. Chem. Chem. Phys.*, **10,** 7121-8.
[41] Roithová, J. and Schröder, D., 2009, *Chemical Reviews*, **110,** 1170-211.
[42] Roth, L. M. and Freiser, B. S., 1991, *Mass Spectrom. Rev.*, **10,** 303-28.
[43] Tonkyn, R. and Weisshaar, J. C., 1986, *J. Am. Chem. Soc.*, **108,** 7128-30.
[44] Weisshaar, J. C., 1993, *Acc. Chem. Res.*, **26,** 213-9.
[45] Ascenzi, D., Franceschi, P., Tosi, P., Bassi, D., Kaczorowska, M. and Harvey, J. N., 2003, *J. Chem. Phys.*, **118,** 2159-63.
[46] Tosi, P., Lu, W., Correale, R. and Bassi, D., 1999, *Chem. Phys. Lett.*, **310,** 180-2.
[47] Tosi, P., Correale, R., Lu, W., Falcinelli, S. and Bassi, D., 1999, *Phys. Rev. Lett.*, **82,** 450-2.
[48] Lambert, N., Kearney, D., Kaltsoyannis, N. and Price, S. D., 2004, *J. Am. Chem. Soc.*, **126,** 3658-63.
[49] Price, S. D., 1997, *J. Chem. Soc., Faraday Trans.*, **93,** 2451-60.
[50] Price, S. D., Manning, M. and Leone, S. R., 1994, *J. Am. Chem. Soc.*, **116,** 8673-80.
[51] Frisch, M. J. T., G. W.; Schlegel, H. B.; Scuseria, G. E.; Robb, M. A.; Cheeseman, J. R.; Scalmani, G.; Barone, V.; Mennucci, B.; Petersson, G. A.; Nakatsuji, H.; Caricato, M.; Li, X.; Hratchian, H. P.; Izmaylov, A. F.; Bloino, J.; Zheng, G.; Sonnenberg, J. L.; Hada, M.; Ehara, M.; Toyota, K.; Fukuda, R.; Hasegawa, J.; Ishida, M.; Nakajima, T.; Honda, Y.; Kitao, O.; Nakai, H.; Vreven, T.; Montgomery, Jr., J. A.; Peralta, J. E.; Ogliaro, F.; Bearpark, M.; Heyd, J. J.; Brothers, E.; Kudin, K. N.; Staroverov, V. N.; Kobayashi, R.; Normand, J.; Raghavachari, K.; Rendell, A.; Burant, J. C.; Iyengar, S. S.; Tomasi, J.; Cossi, M.; Rega, N.; Millam, J. M.; Klene, M.; Knox, J. E.; Cross, J. B.; Bakken, V.; Adamo, C.; Jaramillo, J.; Gomperts, R.; Stratmann, R. E.; Yazyev, O.; Austin, A. J.; Cammi, R.; Pomelli, C.; Ochterski, J. W.; Martin, R. L.; Morokuma, K.; Zakrzewski, V. G.; Voth, G. A.; Salvador, P.; Dannenberg, J. J.; Dapprich, S.; Daniels, A. D.; Farkas, Ö.; Foresman, J. B.; Ortiz, J. V.; Cioslowski, J.; Fox, D. J. (2009) Gaussian, Inc., Wallingford, CT.
[52] Lias, S. G. and Liebman, J. F. In *NIST Chemistry Webbook, NIST Standard Reference Database Number 69*(Eds, Linstrom, P. D. and Mallard, W. G.) National Institue of Standards and Technology, Gaithersburg MD, 20899.
[53] Wittig, C., 2005, *J. Phys. Chem. B.*, **109,** 8428-30.
[54] Zener, C., 1932, *P. Roy. Soc. Lond. A Mat.*, **137,** 696-702.
[55] Landau, L. D., 1932, *Phys. Z. Sowjet.*, **2,** 26.
[56] Olson, R. E., Smith, F. T. and Bauer, E., 1971, *Appl. Opt.*, **10,** 1848-55.
[57] Kearney, D. and Price, S. D., 2003, *Phys. Chem. Chem. Phys.*, **5,** 1575-83.
[58] Price, S. D., 2003, *Phys. Chem. Chem. Phys.*, **5,** 1717-29.
[59] Millie, P., Nenner, I., Archirel, P., Lablanquie, P., Fournier, P. G. and Eland, J. H. D., 1986, *J. Chem. Phys.*, **84,** 1259-69.
[60] Kramida, A., Ralchenko, Y. and Reader, J. (2012) In *NIST Atomic Spectra Database (Version 5.0)* National Institute of Standards and Technology, Gaithersburg, MD.
[61] Hochlaf, M., Hall, R. I., Penent, F., Kjeldsen, H., Lablanquie, P., Lavollée, M. and Eland, J. H. D., 1996, *Chem. Phys.*, **207,** 159-65.
[62] Biemont, E., Hansen, J. E., Quinet, P. and Zeippen, C. J., 1995, *Astron. Astrophys. Sup.*, **111,** 333-46.
[63] Huber, K. P. and Herzberg, G. In *NIST Chemistry Webbook, NIST Standard Reference Database Number 69*(Eds, Linstrom, P. D. and Mallard, W. G.) National Institue of Standards and Technology, Gaithersburg MD, 20899.
[64] Schwarz, H., 2004, *Int. J. Mass Spectrom.*, **237,** 75-105.
[65] Dagdigian, P. J. and Campbell, M. L., 1987, *Chemical Reviews*, **87,** 1-18.

[66] Truhlar, D. G. and Parr, C. A., 1971, *J. Phys. Chem.*, **75,** 1844-60.
[67] Lias, S. G. In *NIST Chemistry Webbook, NIST Standard Reference Database Number 69*(Eds, Linstrom, P. D. and Mallard, W. G.) National Institue of Standards and Technology, Gaithersburg MD, 20899.
[68] Baltzer, P., Wannberg, B., Lundqvist, M., Karlsson, L., Holland, D. M. P., MacDonald, M. A., Hayes, M. A., Tomasello, P. and von Niessen, W., 1996, *Chem. Phys.*, **202,** 185-209.
[69] Brehm, B., Eland, J. H. D., Frey, R. and Küstler, A., 1973, *Int. J. Mass Spectrom. Ion Phys.*, **12,** 213-24.
[70] Aitchison, D. and Eland, J. H. D., 2001, *Chem. Phys.*, **263,** 449-57.
[71] Parkes, M. A., Lockyear, J. F. and Price, S. D., 2013, *Int. J. Mass Spectrom.*, **354,** 39.
[72] Field, T. A. and Eland, J. H. D., 1999, *Chem. Phys. Lett.*, **303,** 144-50.
[73] Burgess, D. R. In *NIST Chemistry Webbook, NIST Standard Reference Database Number 69*(Eds, Linstrom, P. D. and Mallard, W. G.) National Institue of Standards and Technology, Gaithersburg MD, 20899.

Supplementary Information.

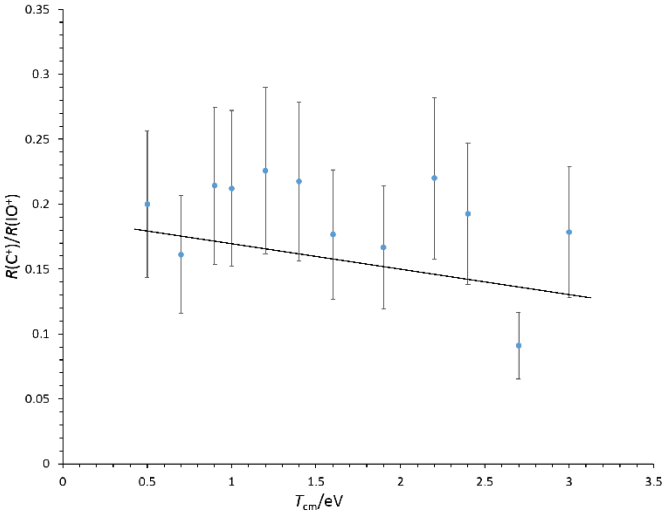

Figure S1 Plot of $R(C^+)/R(IO^+)$ following reactions of I^{2+} with CO. As discussed in the text we would expect this ratio, if the only source of the C^+ ions is the bond-forming reaction, to be effectively constant or only vary slowly over the collision energy range studied. Such behaviour is shown by the data